Electrical stimulation of peripheral nerves induces optical responses via skeletal muscle kinematics

M. Kelley Erb*[a], Debbie K. Chen[b], Angelo Sassaroli[b], Sergio Fantini[b], and Peter R. Bergethon[a]

[a]Boston University School of Medicine, Boston MA, USA 02118;
[b]Tufts University, Medford MA, USA 02155

ABSTRACT

We have previously reported an optical response in human subjects occurring at 100 ms following electrical stimulation of peripheral nerves. In the present study, an animal model has been created to directly investigate the myogenic components of the signal. In addition, experiments have been performed in human subjects to investigate the signal's neuroanatomical specificity, sensitivity to muscle motion, and spatial and spectral features. The results of this work suggest that the observed optical signal derives from stimulus-induced motion associated with muscle contraction and likely contains myological information of clinical value.

Keywords: Near-infrared spectroscopy, peripheral nervous system, skeletal muscle, nerve stimulation, muscle contraction.

1. INTRODUCTION

We have previously reported the existence of an evoked optical response to electrical stimulation of the peripheral nerve measured non-invasively in human subjects[1]. This response constituted a change in the tissue diffuse reflectance of 690 and 830 nm light, with a peak latency between 60 and 160 ms and an amplitude on the order of 0.1%. Initial investigations revealed that signals were wavelength and stimulus-intensity dependent, co-localized to the site of stimulation-induced nerve electrophysiology, and delayed in patients with diabetic neuropathy[2-4]. The timescale of the signals and their wavelength dependence suggested that changes in absorption, rather than scattering, associated with tissue hemodynamic events were likely to underlie those changes. In the present work, we report further studies on the spatial and spectral dependence of these signals, as well as the contribution of stimulus-induced motion and the effect of vascular occlusion, the results of which have been recently published[5, 6]. We also discuss ongoing work aimed at understanding the usefulness of these signals for non-invasively assessing the health of both nerve and muscle.

The current study was designed using both human subjects and an animal model. In human subjects, we have investigated the spatial dependence by measuring the optical signals at twelve locations around a fixed optical collection point during stimulation of the sural nerve. To study the spectral dependence of both optical coupling changes as well as the stimulated response, broadband spectroscopy (650-900 nm) was performed in the wrist using the median nerve. To study the effect of vascular occlusion, a pressure cuff was placed around the upper arm and inflated above venous pressure to achieve venous occlusion, or above systolic arterial pressure to achieve arterial occlusion. To determine the effect of stimulus-induced motion on these optical signals, we compared responses from stimulation of mixed sensory/motor nerves to that of pure sensory nerves, in which the nerve activation could not induce muscle tensioning. Finally, in the animal model, built using the exposed sciatic nerve of a Sprague-Dawley rat, we more directly assessed the contribution of motion by both pharmacologically and surgically disconnecting the nerve from its muscle.

Our measurements show repeatable, spatially dependent optical signals with spectral features that are unaffected by vascular occlusions and are consistent with those of hemoglobin. Moreover, data from both the animal model and human subjects suggest a kinematic origin for these signals. In the animal model, signals were dramatically reduced or completely eliminated following functional disconnection of the nerve from its muscle. In human subjects, pure sensory nerve stimulation failed to elicit a signal, whereas the direct induction of motion via stimulation of mixed nerves generates a large optical response. The temporal characteristics of the current data, as well as those collected previously, are consistent with that of force-velocity measurements made using classical muscle physiology techniques. Together

Optical Tomography and Spectroscopy of Tissue IX,
Edited by Bruce J. Tromberg, Arjun G. Yodh, Mamoru Tamura, Eva M. Sevick-Muraca, Robert R. Alfano,
Proc. of SPIE Vol. 7896, 789609 · © 2011 SPIE · CCC code: 1605-7422/11/$18 · doi: 10.1117/12.875145

with data from ongoing human and animal studies, these data suggest that diffuse optical imaging could be used as a non-invasive tool for investigating muscle kinematics in a variety of clinical scenarios.

2. METHODS

2.1 Stimulation and data acquisition

For both human and animal studies, a clinical nerve conduction velocity / electromyography (EMG) monitor (Carefusion Healthcare, San Diego CA or Cadwell Laboratories, Inc., Kennewick, WA) was used to measure sensory nerve action potentials (SNAPs) and compound muscle action potentials (CMAPs). For the spatial dependence, spectral dependence, and vascular occlusion protocols, recording electrodes were placed in the same area as the optical probe shown in Figs. 1 and 2 to measure the SNAP. Then, the recording electrodes were removed and replaced by the optical probe. The EMG system provided the electrical stimulation at current levels set by the operator. An electrical pulse of 0.1 ms duration, at a repetition rate of 1.5 Hz, was used at the highest level of current below the threshold of any visible skin motion to avoid potential motion artifacts and minimize contributions to the optical data from changes in optical coupling between skin and illumination/collection optical fibers. Stimulation current levels ranged from 5-15 mA. For all animal studies and for the human studies investigating the contribution of motion, SNAPs and CMAPs were recorded continuously during the acquisition of the optical data.

Broadband spectral measurements were made using a xenon arc lamp (Model 6258, Oriel Instruments, Stratford, CT), which was band-pass filtered over the wavelength band 400-1000 nm. Two 2 mm diameter optical fibers served as illumination and collection fibers, respectively, delivering light from the arc lamp to the tissue and collecting light from the tissue to a spectrograph (ModelSP-150, Acton Research Corp., Acton, MA) with a 300 g/mm grating and 700 nm blaze wavelength. We detected spectrally dispersed light with a charged coupled device (CCD) camera (Model DU420A-BR-DD, Andor Technology, South Windsor, CT). The distance between illumination and collector fiber on the tissue was set to 2 cm [Fig. 2(c)]. A LabView program controlled the CCD collection and synchronized the spectral acquisition with the electrical stimulation to collect 30 consecutive spectra following each stimulation pulse, at an acquisition time per spectrum of 18.3 ms.

For all other protocols, optical measurements were made at discrete wavelengths and performed with a commercial near-infrared tissue spectrometer (OxiplexTS, ISS Inc., Champaign, IL) featuring time-multiplexed laser diodes emitting at 690 and 830 nm and detection channels based on photomultiplier tubes (PMT's) [see Fig. 2(a)]. The time resolution for the spatial dependence, vascular occlusion, and mixed versus sensory nerve studies was 20 ms, 40 ms, and 10 ms per data point, respectively. Although the spectrometer is a frequency-domain instrument, we only report continuous-wave intensity data. A portion of the stimulating electrical pulse was coupled to an auxiliary input of the spectrometer to synchronize the electrical stimulation and the acquisition of optical data.

The optical probes for measurements in human subjects consisted of 400 um-diameter illumination optical fibers (coupled to the laser diodes) and 2 mm-diameter collection optical fiber bundles (coupled to the PMT's), arranged according to geometries depicted in Figures 1 and 2. In the spatial dependence study (Fig. 1), the probe consisted of a center detector surrounded by 12 source locations at a radius of 1.5 cm. In the vascular occlusion protocol [Fig. 2(b)] and in the motor versus sensory nerve studies, the probe consisted of a single pair of illumination and collection optical fibers separated by 1.5 cm. For the animal studies, the illumination optical train consisted of an Ocean Optics 400 BIF VIS/NIR bifurcated optical fiber coupled, at its bifurcated end, to the laser diodes of the spectrometer and, at its opposite end, to the 600 μm central fiber of an Ocean Optics QR600- VIS-7-125F backscattering/reflectance probe. A 2 mm-diameter collection optical fiber bundle transmitted light from the tissue back to the PMT of the spectrometer. Both the illumination train and the collection bundle were coupled to the animal using a rectangular light block which prevented both from directly contacting the skin and kept illumination light from reaching the detector without first entering the tissue. The optical probe was built so that 3 different distances could separate the illumination fiber and the collection bundle (3 mm, 8 mm, and 13 mm, respectively), shown in Fig. 3.

2.2 Experiments in human subjects

In human subjects, we have performed studies according to four separate protocols: (1) spatially resolved measurements in response to sural nerve stimulation, (2) broadband spectral measurements in response to median nerve stimulation, (3) measurements made in response to the median nerve stimulation before, during and after vascular occlusion, and (4)

measurements made in response to stimulation of several motion-generating and non-motion-generating nerves. In the first 3 protocols, the stimulus intensity was controlled, as in previous studies, so that no visible skin motion was produced. In the last protocol, we directly compared optical responses elicited with motion-generating stimulation (motor nerves) to those elicited with non-motion-generating stimulation (pure sensory nerves in anatomical compartments without muscles).

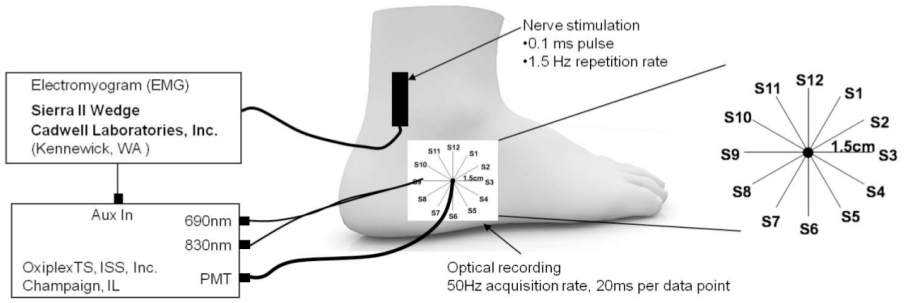

Figure 1. Experimental setup for spatial dependence protocol. A single detection fiber bundle was surrounded by 12 illumination fiber pairs, labeled S1-S12. Sural nerve stimulation was proximal to the site of the optical measurements. The sources were held at each location for 30 seconds.

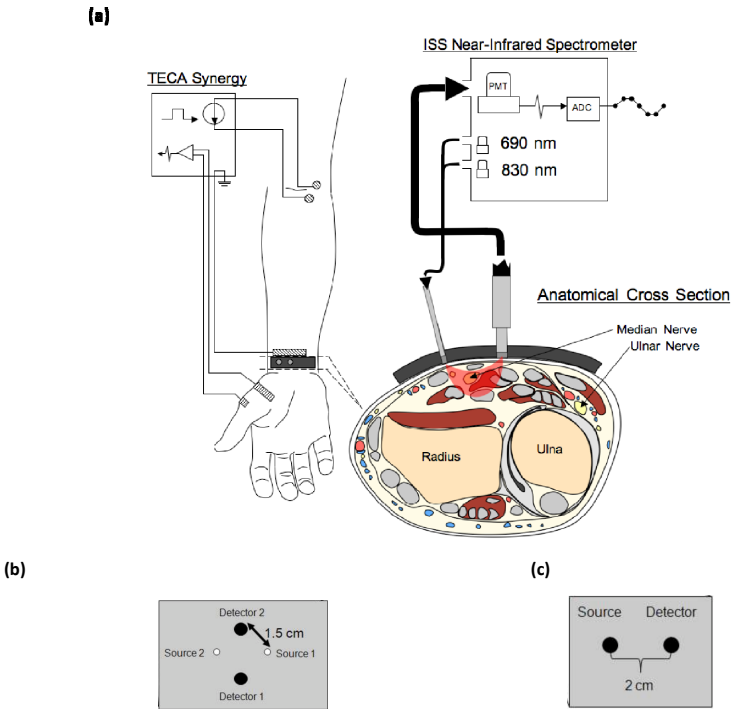

Figure 2. Experimental setup for the human studies. (a) Configuration of the Ag/AgCl electrodes and optical probe while making CMAP measurements of APB during stimulation of the median nerve at the elbow. The anatomical cross section illustrates the location of the median and ulnar nerves in the region of optical interrogation. (b) Probe geometry used for the vascular occlusion protocol. (c) Probe geometry for the spectral dependence protocol.

For the spatial dependence protocol, the set of two illumination optical fibers (one for 690 nm and one for 830 nm) was sequentially placed at each source location (S1-S12) as shown in Fig. 1. The illumination fibers were held at one specific

source location for 30 s before moving to the next location, for a total acquisition time of 6 min for all twelve locations. The collection optical fiber was placed at a fixed location, centered with respect to the sequential source fibers locations. Because of the circular arrangement of the sequential illumination locations S1-S12, we refer to them as 1-12 o'clock positions.

For the spectral dependence protocol, we studied the optical signals in response to nerve stimulation under conditions in which the illumination and collection optical fibers either made contact with the skin (contact configuration) or did not make contact with the skin (non-contact configuration). In the contact configuration, we also measured the change in optical irradiance caused by pushing the collection optical fiber by 125 μm into the skin by means of a finely controlled linear stage. Data were also collected on a tissue-like phantom made of silicon, featuring optical properties similar to those of tissue (μ_a~0.15 cm^{-1}, μ_s'~5 cm^{-1}) in the wavelength band considered in this study (650-900 nm).

The vascular occlusion protocols consisted of 4 phases: 2 minutes with neither nerve stimulation nor vascular occlusion (phase 1), 2 minutes of nerve stimulation but no vascular occlusion (phase 2), 5 minutes of nerve stimulation and vascular occlusion (phase 3), and 5 min of nerve stimulation after the release of vascular occlusion (phase 4).

To study the effect of motion-generating nerve stimulation, CMAPs were acquired in the abductor pollics brevis (APB) muscle and the abductor digiti minimi (ADM) during stimulation of the median nerve, ulnar nerve, and the recurrent branch of the median nerve. To study the effect of non-motion-generating sensory nerve stimulation, antidromic SNAPs were acquired in the medial antebrachial cutaneous nerve (medAC) and the lateral antebrachial cutaneous nerve (latAC) of 4 subjects while measuring the optical response near the recording electrode. Additionally, in the median nerve, orthodromic SNAPs were acquired at the wrist proximal to the carpal tunnel during stimulation of the proper digital branch of the median nerve in the second digit.

2.3 Experiements in the animal model

The animal model was created using the sciatic nerve of the Sprague-Dawley rat. During proximal stimulation of the exposed nerve, optical responses were measured in non-contact mode along its distal course before and after both pharmacological and surgical denervation of lower limb muscles.

All surgical procedures were approved by Boston University School of Medicine's animal care and use committee. Eight animals were anesthetized using 5% isoflurane and then placed in the prone position on a heated surgical bed and maintained anesthetized with 3% isoflurane. The left hind quarter was shaved using an electric trimmer and a chemical depilator (Nair, Church and Dwight Co., Inc., Princeton, NJ) was used to remove the remaining fur. Once prepared for surgery, isoflurane was discontinued and the animal was given an intraperitoneal injection of Ketamine + Xylazine (90 mg/kg and 4 mg/kg, respectively). The animal was then intubated with a 14-gage intravenous catheter and placed on a TOPO Small Animal Ventilator (Kent Scientific, Torrington, CT) in constant pressure mode with the following parameters: respiratory rate; 50 breaths/min, time ratio of inspiratory phase/total respiratory cycle; 30%, peak inspiratory pressure; 13.5 cmH_2O. Blood pressure (BP) and heart rate (HR) were continuously monitored using a common carotid artery catheter and a transducer flushed with heparinized saline. BP and HR data were amplified with multi-purpose transducer amplifier (Harvard Apparatus, Holliston, MA) and then sampled and displayed using a voltage analog input module controlled by a university serial bus (USB) data acquisition system (National Instruments, cDAQ 9172) and LabView software. Once the animal had stabilized on the ventilator and was non-responsive to foot pinch, a skin incision was made just distal to the sciatic notch, where the anterior head of biceps femoris could be blunt dissected from the caudal margin of gluteus maximus, thus exposing the proximal course of the sciatic nerve. The resulting surgical window was held open using an ophthalmologic speculum.

Optical data were acquired from each source-detector distance during approximately 60 nerve stimulations. Before each trial, the optical probe was positioned with a micromanipulator so that the source and detector were equidistant and perpendicular to the course of the nerve. After 1 trial at each source detector distance, a 0.2 mg/kg dose of a clinically used neuromuscular blocking agent, Nimbex (Cisatracurium Besylate), was delivered in a 300 μl bolus via the left common carotid artery catheter. CMAPs were then monitored periodically over the next several minutes to track the action of the drug. Once the CMAP was abolished, another set of optical measurements were made at each source-detector separation. Nimbex belongs to the nondepolarizing class of neuromuscular blocking agents and acts as a competitive antagonist of post-synaptic acetylcholine receptors at the neuromuscular junction. This class of drug has been shown to exhibit affects on the autonomic nervous system[7]. While Nimbex was chosen for its hemodynamic

stability[8], a control experiment was necessary to confirm that changes in the signal on delivery of the drug were related to neuromuscular action and not changes in hemodynamic parameters. In an additional set of animals, a second surgical window was made in the popliteal fossa, distal to both the site of stimulation and the placement of the optical probe. Before the start of the experiment, the tibial and common peroneal nerves were mobilized taking care not to damage major vessels in the space. Following the acquisition of data at each source-detector distance, both nerves were cut distal to their blood supply and a second set of data were acquired at each source detector distance.

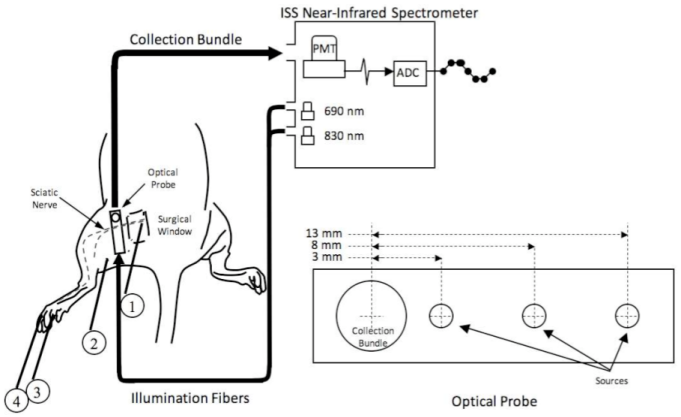

Figure 3. Experimental setup for the animal model. A surgical window was created over the proximal course of the left sciatic nerve in Sprague-Dawley rats. A non-invasive optical probe delivering 690 and 830 nm light at 3 different source-detector separation distances was coupled to the PMT of a frequency-domain spectrometer and oriented perpendicularly to the course of the nerve. 60 x 600 ms epochs, each synchronized to the delivery of a 0.1 ms current stimulus to the exposed nerve (1), were averaged to generate an optical response. Simultaneously, electrophysiological responses to the stimulus were recorded from the plantar muscles of the left foot. (2) ground electrode, (3) active recording electrode, (4) reference electrode.

2.4 Data Analysis

A detailed description of the data processing has been described elsewhere[5, 6]. Briefly, the average change in optical irradiance over N nerve stimulations is written as $<\delta I_{stim}(t)/I(t_0)>$. For spectral measurements of effect of optical coupling, the relative change in irradiance following a change in optical coupling is indicated as $\Delta I_{coupling}/I_0$. For the study of the optical response to nerve stimulation in the vascular occlusion protocol, we report the maximum optical response (with sign) for each individual stimulation, $<\delta I_{stim}(t_{max})/I(t_0)>$, as well as the change in optical irradiance, $\Delta I_{occl}(t)/I_0$, where I_0 is the average irradiance over the two-minute baseline period (phase 1) and $I(t_0)$ is the measured irradiance at the onset of stimulation. This last value reflects the changes in tissue hemoglobin concentration and saturation over the optically probed volume. In section 3.7 we present the results of simultaneous optical and isotonic transducer recordings from isolated muscles in the animal model. Measurements from the isotonic transducer are of changes in muscle length during a twitch and are written as: $\delta x_i(t)/x(t_{0i})$.

3. RESULTS

3.1 Summary

The results are summarized in table 1 and detailed in sections 3.2 – 3.7 and elsewhere[5, 6]. In the animal model, optical signals were completely eliminated following both pharmacological and surgical separation of the nerve from the muscles it innervates. In humans, when the stimulation was of purely sensory nerves, no optical signals could be elicited, even when the electrical stimulation was strong enough to recruit the entire nerve. These three results together suggest that nerve activation alone was insufficient and that motion caused by muscle contraction is necessary to generate an intermediate optical signal. The broadband spectral measurements, made in the distal forearm of human

subjects, indicated that at the time of peak amplitude, the signal had the spectral characteristics of hemoglobin. Moreover, during venous and arterial occlusion, the signals responded differently than the background tissue optical properties. For example, during arterial occlusion, the background tissue irradiance of 830 nm light increased while that of 690 nm light decreased, indicating hemoglobin desaturation in tissue capillary beds. The amplitude of both 690 nm and 830 nm nerve-stimulation induced signals, however, remained identical. These two results suggest that while blood containing structures likely underlie these signals, they are most likely due to large vessels rather than small capillary beds. Finally, we sought to determine the nature of the motion causing these signals. The spatially resolved measurements indicated that displacements of these vessels are more likely than rapid dilation or constriction. This is because the polarity and amplitude were found to vary smoothly over space, with positive-going signals observed in some locations and negative-going signals in others. Rapid vascular dilations and constrictions would not have this effect. They would have the same polarity in all locations.

Table 1: A summary of the results and their implications for the biological origin of the optical signal

		RESULTS	
Question	Protocol	Results	Conclusion
Contribution of Motion	Neuromuscular Block (animal model)	Signals are lost following block and return with washout of the drug	Contractile motion induced by nerve stimulation is necessary and sufficient to generate an intermediate signal
	Surgical Denervation (animal model)	Nerve transection also eliminates the optical signal	
	Sensory vs. Mixed Nerves	Sensory Nerves: No Signal Mixed Nerves: Large Signal	
Structures involved	Spectral Dependence	At the time of peak signal amplitude, the spectral nature of the signal reflects that of hemoglobin	Motion of blood-containing structures dominate the signal
	Vascular Occlusion	During occlusion, changes to the Signal are not the same as changes to the background tissue optical properties	Signal is not derived from tissue capillary beds, which determine background optical properties
Dilation or Displacement	Spatial Dependence	Signals are positive-going in some locations and negative-going in others	Displacement of a large vessel could account for the signal, but not dilation, which would cause signals to be either always positive or always negative

3.2 Spatial dependence

Figure 4 shows both the probe geometry as well as a representative result from subject 1 for the spatial dependence protocol. Across all 5 subjects the direction of the optical response was positive at locations in the upper right quadrant (i.e. S1-S3) and flat or negative in the other 3 quadrants. This result is consistent with the displacement of a blood vessel within the optically probed region. It is not consistent with the hypothesis that vessels are either rapidly dilating or constricting, in which case the signal would always be either positive or negative, respectively. These findings are also consistent with the anatomy of this region. The sural nerve travels obliquely beneath the lateral malleolus as it enters the dorsal aspect of the foot from the lower leg. Nutrient vascular supply to peripheral nerves includes branches from adjacent epineurial, fasciocutaneous, or muscular arteries, all of which anastomose to form a continuous longitudinal plexus that travels with the nerve.

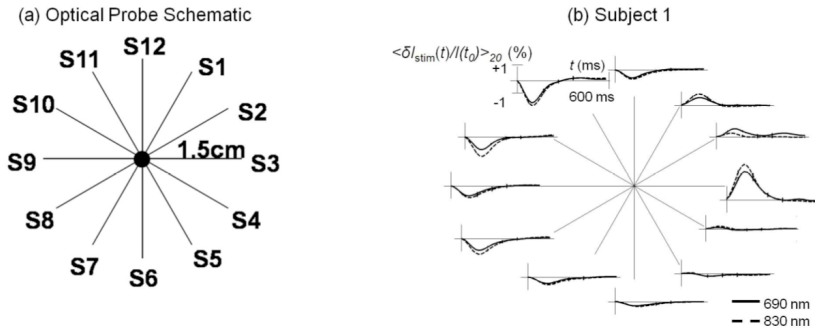

Figure 4. (a) Schematic diagram of the optical probe for spatially resolved measurements; (b) Optical responses to right sural nerve stimulation for the twelve source-detector pairs measured on subject 1.

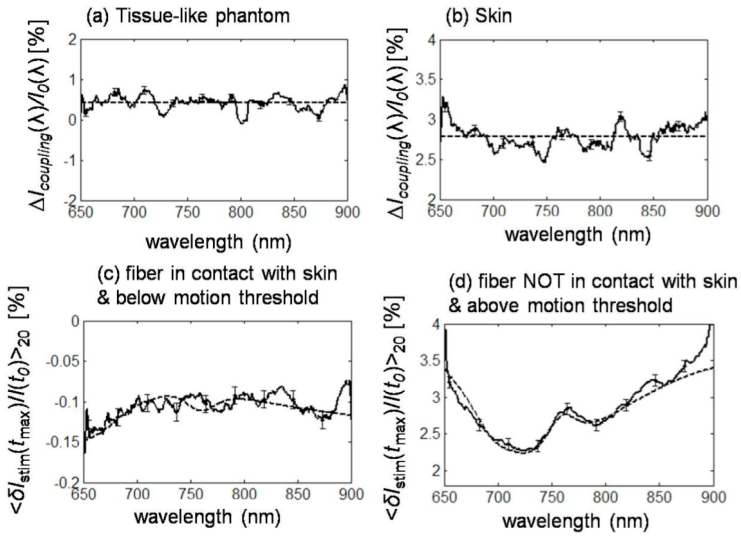

Figure 5. Broadband spectra of optical signals measured (a) on a tissue-like phantom as a result of pushing the detector fiber by 250 μm into the phantom in a contact configuration, and on subject 6 (b) as a result of pushing the detector fiber by 125 μm into the skin in a contact configuration. Broadband spectra are also shown at the point of maximal optical response to median nerve stimulation under conditions of (c) fiber-skin contact and no visible hand motion, and (d) no contact between optical fiber and skin, and visible stimulation-induced hand motion.

3.3 Spectral dependence

We studied the spectral dependence of optical coupling effects by acquiring broadband spectra before and after lowering the optical probe into contact with the subject using a finely tuned linear stage. Changing the optical coupling induced optical irradiance changes with a flat spectral dependence and an average value of 0.42 ± 0.09% in the tissue phantom case [flat dashed line in Fig. 5(a)] and 2.78 ± 0.06% in the *in vivo* case [flat dashed line in Fig. 5(b)]. In addition, the lower panels of figure 5 show that the optical response to median nerve stimulation, as a function of wavelength, reflects the spectral signature of hemoglobin in the case where the fibers were not in contact with the skin [c.f. Fig. 5(d)].

3.4 Effect of vascular occlusion

The results of vascular occlusion are shown in figure 6. The experiment consisted of 4 phases for both venous and arterial occlusion. Phase 1 is a baseline control period where the pressure cuff was deflated and no stimulation took place. During phase 2, when stimulation began but the pressure cuff remained deflated, the background tissue irradiance

was unaffected (figure 6, upper traces). Negative going optical responses, however, were observed in both experiments (figure 6, lower traces) and had an amplitude ranging from -0.2% to -0.5%. During phase 3, when the cuff was inflated, the background tissue irradiance changed depending on the type of occlusion. For venous occlusion, the irradiance of both wavelengths decreased, consistent with an increase in total blood volume corresponding to increases in both [Hb] and [Hbo2]. During Arterial occlusion, the irradiance of 690 nm light decreased and that of 830 nm light increased, consistent with the deoxygenation of hemoglobin associated with an increase in [Hb] a decrease in [Hbo2]. The stimulated responses during this phase, however, did not follow the changes observed in the background tissue. The response amplitude for both wavelengths during venous occlusion decreased (i.e. is less negative or dampened). During the arterial occlusion, however, the response amplitude of both wavelengths increased slightly (i.e. became more negative). During phase 4, both the background irradiance and the stimulated response returned to pre-occlusion baseline levels for both arterial and venous occlusion.

The most striking result of these experiments is that arterial occlusion had opposite effects on the background tissue irradiance of the different wavelengths but the same effect on their maximum response during stimulation. This suggests that the optical response to nerve stimulation does not derive from capillary hemoblobin, which provides the dominant contribution to $\Delta I_{occl}(t)/I_0$.

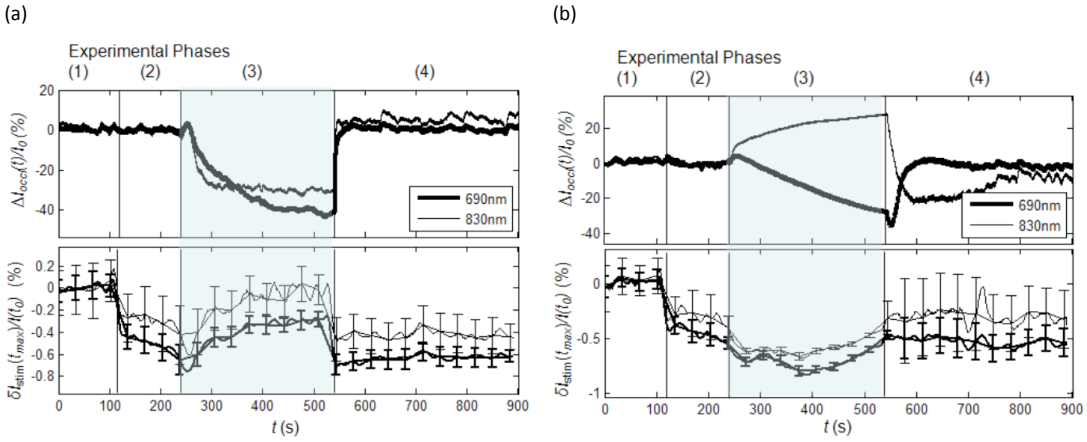

Figure 6. (a) results obtained from subject 6 during venous occlusion. (b) results obtained from subject 6 during arterial occlusion. The numbers above each panel correspond to the respective phases of the experiment (see text).

3.5 Mixed nerve stimulation versus sensory nerve stimulation

Figure 7(a), top panel, shows a supramaximal electrophysiological response measured in the APB and demonstrates that the entire muscle was recruited, which produced large amplitude motion of the thumb. The amplitude (~10%) of the corresponding optical response is 2 orders of magnitude larger than that of signals described previously[1], though the temporal and spectral features are comparable, suggesting a similar biological origin. Similar results were obtained during stimulation of both the ulnar nerve and the median nerve at the elbow (Figure 7(a)). While the median nerve does travel in the optically probed region, the ulnar nerve does not. However, both of these nerves do innervate muscles whose tendons are located in the distal forearm beneath the optical probe. In all subjects, stimulation under each of these three conditions resulted in large amplitude signals demonstrating that optical measurements at the wrist are sensitive to motion induced by nerves which are both within and outside the region of optical interrogation.

Figure 7(b) shows the results from subject 2 during sensory nerve activation of the median nerve, medial antebrachial cutaneous nerve, and lateral antebrachial cutaneous nerve. In each case, despite the presence of a robust electrical signal in the optically probed region, no optical response was detected. In all other subjects, no optical response was observed in any of the sensory stimulation conditions.

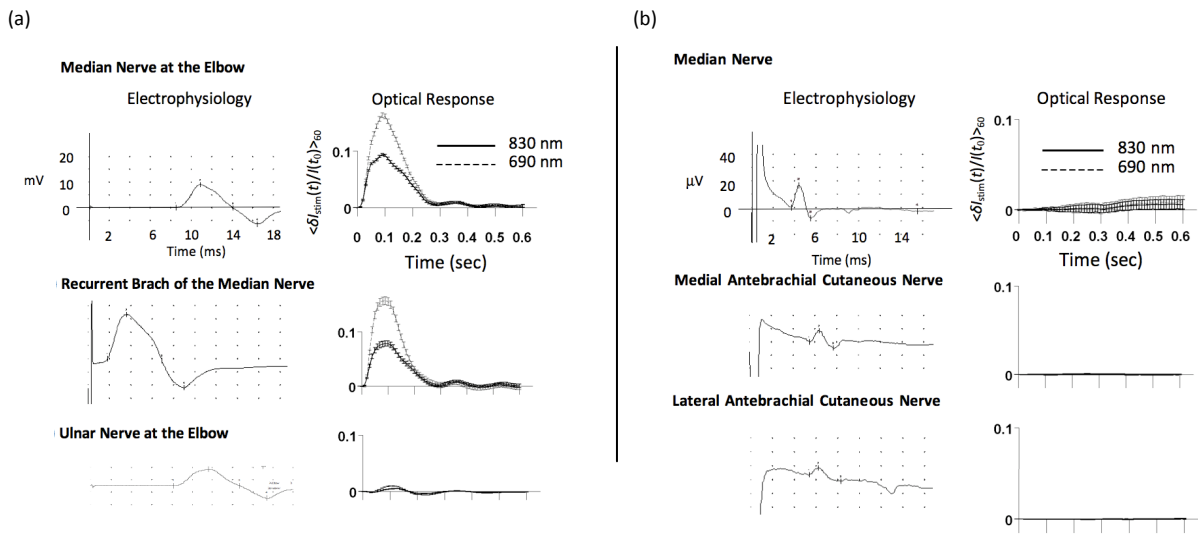

Figure 7. Optical responses at the wrist during stimulation of mixed nerves in subject 2. (a, top panel) CMAP generated in APB (left) and the corresponding optical response (right) during stimulation of the median nerve at the elbow. (a, middle panel) CMAP and corresponding optical trace during stimulation of the recurrent branch of the median nerve in the palm. (a, bottom panel) CMAP and corresponding optical response during stimulation of the ulnar nerve at the elbow. Differences in the latency-to-onset of the electrophysiological response between stimulation at the elbow and at the recurrent branch of the median nerve reflect the increased distance (~20 cm) over which the nerve impulse must travel before depolarizing the muscle. (b) Optical data during sensory nerve stimulation in subject 2. (top panel) Median nerve SNAP measured at the wrist during stimulation of the 2nd digit and the corresponding optical data. (middle panel) Medial antebrachial cutaneous SNAP and corresponding optical data. (bottom panel) Lateral antebrachial cutaneous SNAP and corresponding optical data

3.6 Animal model: effect of neuromuscular block and surgical denervation

Figure 8 shows a typical plantar muscle action potential and the corresponding optical time-trace obtained from the middle source-detector separation in the animal model. In general, optical signals obtained from the rodent hind limb are faster than those obtained from the human forearm, reaching peak amplitude between 30 and 40 ms post-stimulus. The amplitude of the signal was on the order of 1-5% and this was not affected by changing the source-detector separation distance.

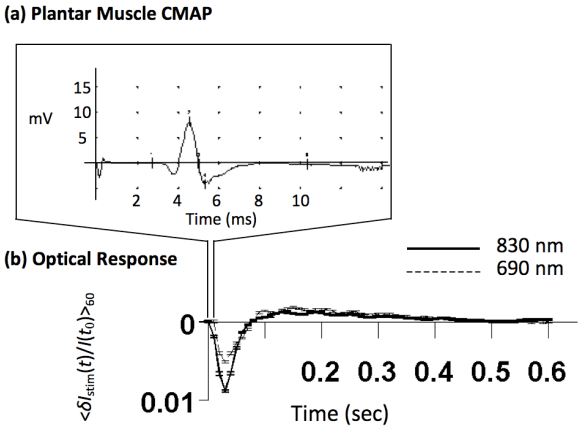

Figure 8. Typical results from middle source-detector separation in the animal model. (a) A plantar muscle action potential. (b) Signals generated in the lower limb of the Sprague-Dawley rat are faster than signals generated in human subjects.

The direction of the signal (positive vs. negative irradiance changes) varied, both within a single animal (at different source-detector separations) or between animals. This finding is in agreement with signals generated in human subjects both in this and previous work [6]. In all 5 animals, a 0.2 mg/kg intra-arterial dose of Cisatracurium Besylate dramatically reduced, or completely eliminated the stimulation-induced signals, Fig. 9 (b).

In 3 animals, optical responses were reduced by an order of magnitude though none-the-less remained statistically significant at several source-detector separations. Animals given an intravenous bolus of Cisatracurium at doses between 1.5 and 6 ED_{95} have been shown to begin spontaneously recovering after as little as 20 minutes [9]. In this study, boluses were being delivered intra-arterially; a route that could speed the clearance of the drug. Indeed, in one animal, following an approximately 15 minute washout period, the return of the plantar muscle CMAPs was associated with a dramatic return of the optical signal (Figure 9 (c)). This apparent dose-response relationship was later confirmed in a 6th animal in which signals were present following a 0.100 mg/kg dose but eliminated following a 0.6 mg/kg dose. This result suggests, though does not confirm, a correlation between the amplitude of the optical response and the percentage of recruited muscle fibers.

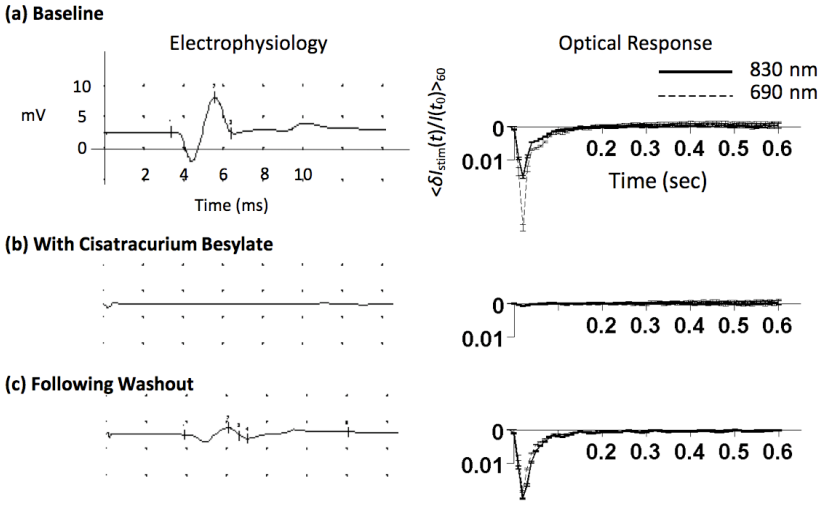

Figure 9. The effect of Cisatracurium Besylate on signals generated in the rat. (a) Signals from the middle source-detector separation in one of the rats prior to delivery of the drug. (b) Optical traces from the same rat following drug delivery. (c) Following a 15 minute washout period, both the electrophysiological and optical response returned.

In an additional set of animals, the two divisions of the sciatic nerve (tibial and common peroneal) were surgically transected in the popliteal fossa. This manipulation produces the same functional disconnection of nerve from muscle while avoiding potential hemodynamic side affects associated with acetylcholine receptor blockade. In agreement with the pharmacological results, surgical disconnection of the nerve from the muscle eliminated nerve-stimulation induced optical responses at each source-detector separation.

3.7 Animal model: Isolated muscles, preliminary results

We have recently begun to investigate the potential of these diffuse optical measurements to directly measure muscle contractile physiology. Figure 10 shows the results from one Sprague-Dawley rat in which the surgical methods described above were extended to include isolating the gastrocnemius muscle and the soleus muscle from their surrounding tissues, with the nerve and blood supply left intact. The distal tendons were separated from the foot and attached to an isotonic transducer, which was secured from the opposite direction by a spring. The nerve was then stimulated at frequencies below and above the fusion frequency for tetanus while measuring optically directly from the

surface of the muscle (4, 6, and 15 hz, in panels a, b, and c, respectively). The upper traces are records from the isotonic transducer for both muscles and the lower traces are the optical measurements. Interestingly, even in this preliminary set of data, the two muscles can be distinguished on the basis of their optical responses. Using both this animal model and a variety of human clinical populations, we are continuing to investigate the sensitivity and specificity of this tool for detecting changes muscle contractile physiology that may evolve in healthy and diseased muscle.

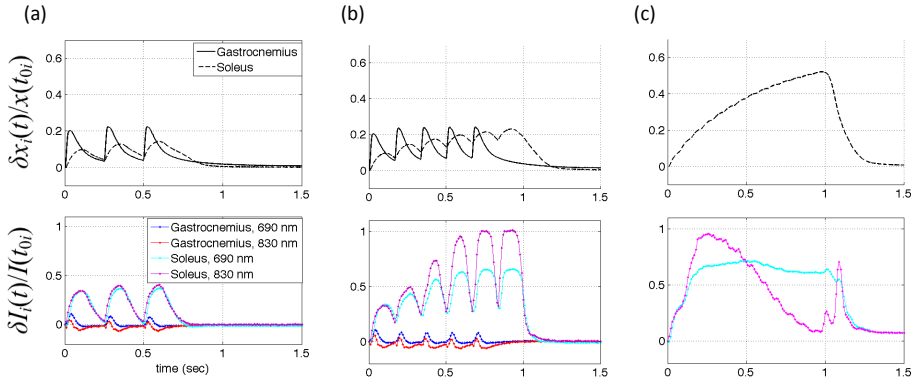

Figure 10. NIRS optical signals map time course of whole muscle force and length during 4, 6, and 15 Hz stimulation. The upper graph of each panel shows relative change in muscle length recorded by the isotonic transducer and the lower graphs each are optical data recorded at both 690 nm and 830 nm. Panels (a) and (b) both Soleus (slow twitch) and Gastrocnemius (fast twitch) for 4 Hz and 6 Hz, respectively. Panel (c) Soleus only, demonstrating the effect of fused tetanus (15 Hz).

4. DISCUSSION

The optical signals reported here were generated by peripheral nerve stimulation and detected in anatomical regions that fall into two categories, 1) those containing mostly muscle tissue (the upper leg in the animal model), and 2) those containing few or no muscles (the human distal forearm and lateral ankle). In the compartments that do not contain muscles, the results of the spatially and spectrally resolved measurements strongly suggest that motion of blood-containing structures account for these signals. In the lateral aspect of the ankle, the major blood containing structures include the small saphenous vein and the fibular artery, which travel with the continuation of the sural nerve. The sural nerve itself is also well supplied with vessels. These three structures are mechanically linked by their investing fascia. Thus, any mechanical tensioning that acts on the nerve will also put these vessels into motion, and this likely explains the signals generated in this region. In the distal forearm, however, the principle blood containing structures are the ulnar and radial arteries, which do not travel with the median nerve. The median nerve, however, like the sural nerve, has a rich epineurial and endoneurial vascular network. Blood in this network, therefore, likely constitutes the imaging contrast agent and therefore changes to median nerve blood supply might be reflected in changes to these optical signals. In diabetes, for instance, microangiopathies are considered to play a role in the pathogenesis of diabetic polyneuropathy[10]. These signals may prove a useful non-invasive assessment tool for the vascular health of peripheral nerves.

We have also generated robust signals in optically probed regions that are comprised primarily of muscle tissue. These signals have a time course that is highly consistent with the time course of muscle contraction. Preliminary results obtained from isolated muscles in our animal model demonstrate that these signals can distinguish muscles of different contraction times and suggest that this tool could be used to follow changes in their contractile properties.

In our initial investigations, great care was taken to control the level of stimulation so that the investigator could not detect visible skin motion. The signal amplitudes under these conditions were small (~0.2% - 0.5%) but none-the-less robust and repeatable. This high sensitivity suggests that diffuse optical imaging might be capable of detecting the contraction events of single motor units, which would make it valuable for studying neuromuscular changes that accompany aging and disease[11], especially in locations inaccessible to force transducers.

ACKNOWLEDGMENTS

This work is supported by National Institutes of Health (NIH) Grants R01-NS059933, National Institute on Aging (NIA) T32-001, T32-AG00277, and by CIMIT/U.S. Army Medical Acquisition Activity (USAMRAA) funding under cooperative agreement no. W81XWH-07-2-0011

REFERENCES

[1] Y Tong, JM Martin, A Sassaroli *et al.*, "Fast optical signals in the peripheral nervous system," J Biomed Opt, 11(4), 044014 (2006).

[2] DK Chen, Y Tong, A Sassaroli *et al.*, "Fast optical response to electrical activation in peripheral nerves - art. no. 643104," Multimodal Biomedical Imaging II, 6431, 43104-43104 43100 (2007).

[3] S Fantini, DK Chen, JM Martin *et al.*, "Near-infrared signals associated with electrical stimulation of peripheral nerves," Proc SPIE, 7174, (2009).

[4] S Fantini, DK Chen, JM Martin *et al.*, "Optical characterization of near-infrared signals associated with electrical stimulation of peripheral nerves," Proc SPIE, 7174, 717401 (2009).

[5] MK Erb, DK Chen, A Sassaroli *et al.*, "Diffuse optical signals in response to peripheral nerve stimulation reflect skeletal muscle kinematics," Biomedical Optics Express, 1(3), 943-954 (2010).

[6] DK Chen, MK Erb, Y Tong *et al.*, "Spectral and spatial dependence of diffuse optical signals in response to peripheral nerve stimulation," Biomedical Optics Express, 1(3), 923-942 (2010).

[7] S Virmani, DK Tempe, V Datt *et al.*, "Effect of muscle relaxants on heart rate, arterial pressure, intubation conditions and onset of neuromuscular block in patients undergoing valve surgery," Ann Card Anaesth, 9(1), 37-43 (2006).

[8] A Esmaoglu, A Akin, A Mizrak *et al.*, "Addition of cisatracurium to lidocaine for intravenous regional anesthesia," J Clin Anesth, 18(3), 194-7 (2006).

[9] C Chen, N Yamaguchi, and F Varin, "Dose-dependency of pharmacokinetic/pharmacodynamic parameters after intravenous bolus doses of cisatracurium," Br J Anaesth, 101(6), 788-97 (2008).

[10] M Theriault, J Dort, G Sutherland *et al.*, "Local human sural nerve blood flow in diabetic and other polyneuropathies," Brain, 120 (Pt 7), 1131-8 (1997).

[11] KM Chan, TJ Doherty, and WF Brown, "Contractile properties of human motor units in health, aging, and disease," Muscle & Nerve, 24(9), 1113-1133 (2001).